Noise Characteristics of Current Mirror Sinks/Sources

ALBERTO BILOTTI, SENIOR MEMBER, IEEE, AND EDUARDO MARIANI

Abstract—General expressions of the limiting and excess noise currents generated by a current mirror sink/source are derived. The analysis, restricted to low and audio frequencies, shows the effect of the transistor base resistance and the noise reduction due to the external emitter degeneration.

By means of a computer-aided design (CAD) analysis, spectral density frequency plots are computed, and the total noise content in the audio band calculated for the case of a typical $1/f$ excess noise generator. The noise characteristics of other current source topologies are compared and shown to be quite similar to the basic current mirror.

Noise measurements of current mirrors implemented with IC transistor pairs showed a good correlation with the previous analytical and CAD results.

I. Introduction

THE DIODE-TRANSISTOR current mirror sink/sources are useful building blocks widely used in monolithic analog IC's. Since it was first proposed by Widlar in 1965 [1], the matching and temperature properties [2], [3], the small signal characteristics [4], and methods of calculation [5], [6] have been reported. In order to improve the matching accuracy, the temperature desensitization and/or the output resistance, improved versions of the original current mirror have also been proposed [7]-[10].

The purpose of this paper is to investigate the noise characteristics of the basic current mirror source,[1] particularly for low and audio frequencies. In fact, the dc output current provided by the source is always contaminated with an additional noise current I_{on} generated by the active and passive components. This can be particularly important in low level stages where current sources are used as biasing means, balance to unbalance converters, active loads, etc., a typical example being the current mirror source at the input of the Norton amplifiers [11], [12]. Noise may be also undesirable in other applications as in variable gain quads and high performance analog multipliers where the current mirror topology is used for linearization purposes.

Fig. 1 shows a unity-gain current mirror source where the reference current I_i is fed to a diode-connected transistor Q_1 and the output current I_o is provided by a matched output transistor Q_2. The two emitter degeneration resistors R_E, often used to improve the matching or to increase the output resistance, will be shown to play an important role in the circuit noise behavior.

In most applications the source resistance of the reference generator I_i is much higher than the input resistance of the current mirror and can be neglected. Therefore, the circuit

Manuscript received March 26, 1975; revised July 9, 1975.

The authors are with the Department of Electronics, Faculty of Engineering, University of Buenos Aires, Buenos Aires, Argentina.

[1] Since the difference between a sink and a source involves only a change in the polarity, the term source will be used in the text to indicate either one.

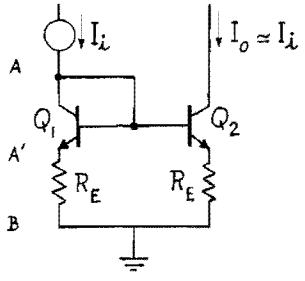

Fig. 1. Basic unity-gain current mirror with emitter degenerating resistance R_E.

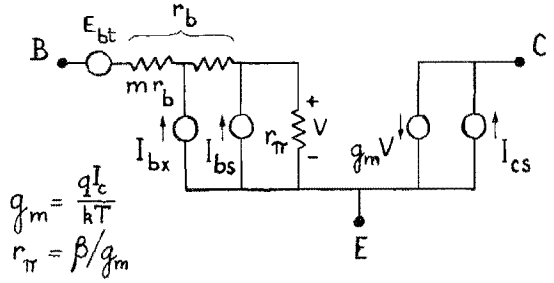

Fig. 2. Simplified hybrid π model. Current sources I_{cs} and I_{bs} account for the output and input shot noise, I_{bx} for the excess noise, and E_{bt} for the thermal noise due to r_b. Resistance mr_b is the effective base resistance associated to the excess noise generator.

noise performance can be evaluated by analyzing the behavior of the output noise current I_{on} with a noiseless reference current I_i.

The output noise current can always be split into a flat spectrum limiting component I_{ol} due to shot and thermal noises and a frequency dependent excess noise component I_{ox} such that

$$I_{on} = (I_{ol}^2 + I_{ox}^2)^{1/2}. \tag{1}$$

When these components are considered separately, the relative effect of changes in the circuit variables can be analyzed regardless of the particular excess noise spectrum and noise bandwidth. Most of the analytical work in this paper deals with the individual circuit behavior of I_{ol} and I_{ox}.

In order to reduce the number of variables and simplify the interpretation of the analytical results, most of the calculations and discussions will be restricted to the case of unity-current ratio and identical transistors shown in Fig. 1. The general case of current mirrors with variable current ratios and scaled emitter areas is treated in the Appendix.

II. Transistor Noise Model and Assumptions

As the analysis is restricted to the audio frequency range, the transistors will be modeled by the simplified frequency independent hybrid π circuit shown in Fig. 2. As all transfer functions to be derived in the circuit of Fig. 1 will also be

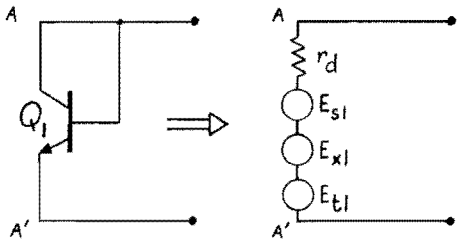

Fig. 3. Equivalent noise circuit of a diode-connected transistor. The internal resistance r_d and the shot, excess, and thermal equivalent noise voltages E_{s1}, E_{x1}, and E_{t1} are given by (9)–(12) in the text.

frequency independent, the noise sources in Fig. 2 are assumed, for simplicity, to represent rms values for a given bandwidth $(f_2 - f_1)$.

The noise current generators I_{bs} and I_{cs} show the full shot noise of the base and collector bias currents I_B and I_C, the current generator I_{bx} accounts for any excess noise at the transistor input, and the noise voltage E_{bt} for the base resistance thermal noise. For general purposes, the excess noise generator is shown to be affected by a fraction m of the total base resistance r_b.

For a given noise bandwidth $(f_2 - f_1)$ the four noise generators of Fig. 2 are [13]

$$I_{bs} = [2qI_B(f_2 - f_1)]^{1/2} \tag{2}$$

$$I_{cs} = [2qI_C(f_2 - f_1)]^{1/2} \tag{3}$$

$$I_{bx} = \left[\int_{f_1}^{f_2} S_x(f)\,df\right]^{1/2} \tag{4}$$

$$E_{bt} = [4kTr_b(f_2 - f_1)]^{1/2} \tag{5}$$

where $S_x(f)$ is the spectral density (amperes square per hertz) of the excess noise current generator and the other symbols have the conventional meaning.

The excess noise is frequency dependent, dominant at low frequencies, and generally due to different noise mechanisms. Two types of excess noise are usually found in monolithic transistors, the flicker or $1/f$ noise, and the burst noise [14], [15] with typical spectra given by

$$(S_x)_{1/f} = \frac{C_a I_B^{\gamma a}}{f} \tag{6}$$

$$(S_x)_{\text{burst}} = \frac{C_b I_B^{\gamma b}}{1 + \left(\frac{\pi f}{2a}\right)^2} \tag{7}$$

where the constants C, a, and γ depend on the transistor type and the particular process.

Although exact modeling of the excess noise may require two or more different noise generators with different m's, each one can be treated as the unique noise generator I_{bx}, shown in Fig. 2, and their mean-square contributions to I_{on} added.

For the noise analysis of Fig. 1, we further assume that: transistors are identical and all noise sources are uncorrelated; $I_o = I_i$; $m\beta \gg 1$; $\beta \simeq \beta_{dc} \gg 1$.

The assumption of equal dc and ac forward current transfer gains and (2) and (3) provide a useful relation between both shot noise sources

$$I_{cs}/I_{bs} = \beta^{1/2}. \tag{8}$$

III. Analysis

In order to derive an expression of the output noise current I_{on} as a function of the circuit variables in Fig. 1, both transistors are substituted by their equivalent circuit shown in Fig. 2. Since the complete circuit is linear, by superposition each noise generator can be treated independently. The procedure is simplified by calculating first the equivalent open circuit shot and excess noise voltages of the diode-connected transistor Q_1, and then the equivalent input noise voltages of the common-emitter transistor Q_2. The final equivalent noise circuit shown in Fig. 5 has five uncorrelated noise voltages at the input of Q_2 and allows straightforward calculation of the collector noise current.

Equivalent Noise Voltages of Q_1

Solving the hybrid π model of Fig. 2 for the case of the diode-connected transistor Q_1, the small signal equivalent circuit of Fig. 3 is found, where the diode internal resistance r_d and the open circuit shot, excess, and thermal noise voltages E_{s1}, E_{x1}, and E_{t1} are shown to be

$$r_d = r_e + r_b/\beta \tag{9}$$

$$E_{s1} = I_{cs}(r_e^2 + r_b^2/\beta)^{1/2} \tag{10}$$

$$E_{x1} = I_{bx}(r_d - mr_b) \tag{11}$$

$$E_{t1} = E_{bt} \tag{12}$$

where

$$r_e = \frac{kT}{qI_o} \simeq \frac{kT}{qI_i} \simeq 1/g_m. \tag{13}$$

The shot noise voltage E_{s1} has been obtained by the rms addition of the contributions due to I_{bs} and I_{cs} and the elimination of I_{bs} by means of (8). Note that the excess noise can be fully cancelled for $r_d = mr_b$.

Equivalent Input Noise Voltages of Q_2

To evaluate the noise contribution of Q_2 in Fig. 1, the diode-connected transistor can be substituted by a noiseless diode with internal resistance r_d. Therefore, Q_2 operates with a source resistance $R_s = r_d + R_E$ at the input port AB. Pro-

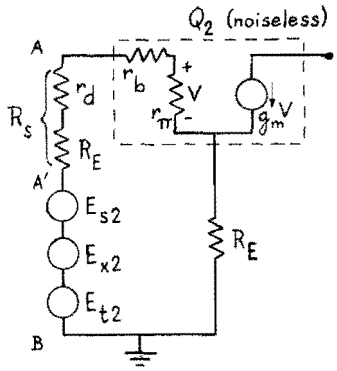

Fig. 4. Equivalent noise circuit of a common-emitter transistor with source and emitter resistances R_S and R_E. The equivalent input noise voltages E_{s2}, E_{x2}, and E_{t2} are given by (14)-(16) in the text.

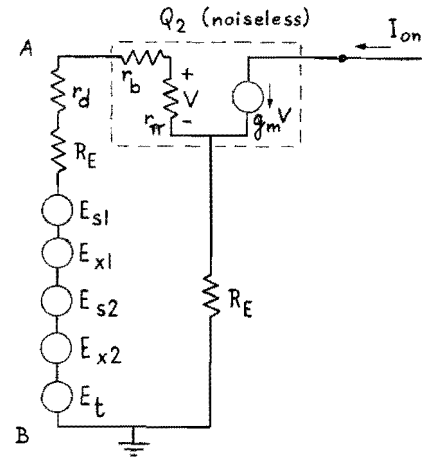

Fig. 5. Equivalent noise circuit of the current mirror of Fig. 1. The five uncorrelated equivalent input noise voltages represent the shot and excess noise of both transistors and the total thermal noise of the base and emitter degenerating resistances.

ceeding as before, the noise equivalent circuit of Fig. 4 is found, where the shot, excess, and thermal equivalent input noise voltages E_{s2}, E_{x2}, and E_{t2} are given by

$$E_{s2} = I_{cs}[(r_e + r_b + R_E + R_s)^2/\beta + r_e^2]^{1/2} \tag{14}$$

$$E_{x2} = I_{bx}(mr_b + R_E + R_s) \tag{15}$$

$$E_{t2} = E_{tb} \tag{16}$$

where

$$R_s = r_d + R_E. \tag{17}$$

The collector noise current due to any of the equivalent noise generators is given by the input noise voltage times the circuit transconductance G_m,

$$G_m = [r_e + (R_s + r_b)/\beta + R_E]^{-1}. \tag{18}$$

Expressions (14)-(18) are also applicable to any common-emitter stage with emitter degeneration and source resistances R_E and R_s, respectively.

Output Noise Current of the Current Mirror

Using the equivalent circuits of Figs. 3 and 4 the final noise equivalent circuit of the current mirror is obtained. Fig. 5 shows that the total noise can be accounted for by five uncorrelated noise voltages at the input of Q_2. They are the previously calculated shot and excess noise voltages of Q_1 and Q_2, and the total thermal noise voltage E_t. The total thermal noise voltage is not only due to the transistor base resistances but also to the thermal noise generated by the emitter degeneration resistors R_E, hence

$$E_t = [4kT(2r_b + 2R_E)(f_2 - f_1)]^{1/2}. \tag{19}$$

Using (3) and recalling that $I_C \simeq I_o = kT/qr_e$, (19) can be written as a function of I_{cs}

$$E_t = 2I_{cs}[r_e(r_b + R_E)]^{1/2}. \tag{20}$$

Each one of the noise voltages shown in Fig. 5 times the circuit transconductance G_m gives rise to a noise current component at the output. These five noise currents can be better resolved into a limiting noise current I_{ol} and an excess noise current I_{ox}, where the first includes both the shot and the thermal flat spectrum noises. The total output noise current is then

$$I_{on} = (I_{ol}^2 + I_{ox}^2)^{1/2} \tag{21}$$

where

$$I_{ol} = (E_{s1}^2 + E_{s2}^2 + E_t^2)^{1/2} G_m \tag{22}$$

$$I_{ox} = (E_{x1}^2 + E_{x2}^2)^{1/2} G_m. \tag{23}$$

In order to simplify the notation, r_b and R_E will be normalized with respect to r_e by means of parameters b and d,

$$b = r_b/r_e, \quad d = R_E/r_e. \tag{24}$$

Using the noise voltage expressions (10), (11), (14), (15), and (20) together with (9), (17), and (18), and eliminating r_b and R_E through (24), expressions (22) and (23) yield, after some manipulation,

$$I_{ol} = \sqrt{2}\, I_{cs} \frac{[1 + 2b + b^2/\beta + 2d(1 + b/\beta) + 2d^2/\beta]^{1/2}}{1 + b/\beta + d} \tag{25}$$

$$I_{ox} = \sqrt{2}\, I_{bx} \frac{[1 + (mb)^2 + 2d(1 + mb) + 2d^2]^{1/2}}{1 + b/\beta + d}. \tag{26}$$

These are the final general expressions of the limiting and excess noise components of the output noise current generated by the current mirror of Fig. 1. They are particularly useful to investigate the noise behavior at constant output current I_o and bandwidth. Under these conditions, the shot and excess noise sources I_{cs} and I_{bx}, as well as r_e, are constant and the fractions in (25) and (26) give, through parameters b and d, the functional dependence on the transistor base and emitter degeneration resistances. Furthermore, I_{cs} is independent of β at constant output, although I_{bx} is not due to its dependence on I_B through (4), (6), or (7).

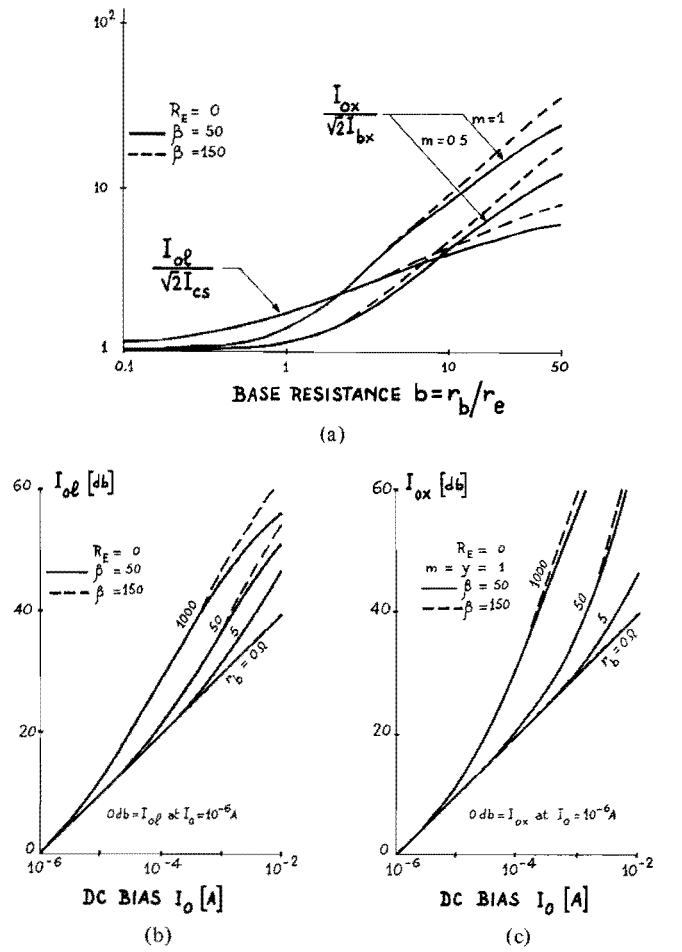

Fig. 6. Normalized limiting and excess output noise current of the basic current source of Fig. 1 as a function of (a) the base resistance parameter $b = r_b/r_e$, (b) and (c) the dc bias current.

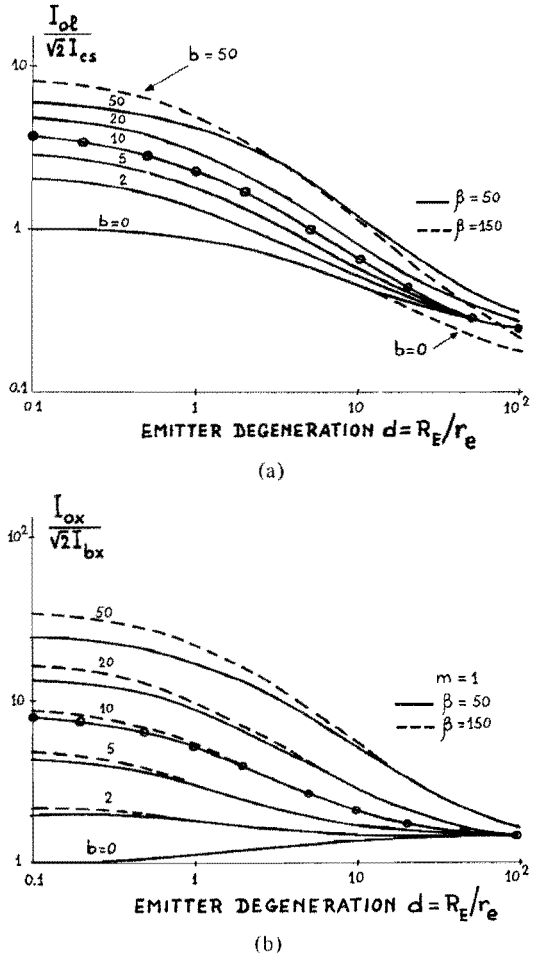

Fig. 7. (a) Normalized limiting noise as a function of $b = r_b/r_e$ and $d = R_E/r_e$ calculated from (25). (b) Normalized excess noise as a function of b and d for $m = 1$, calculated from (26). The dots on the $b = 10$ curves are the exact computer-derived values for $b = 10$ and $\beta = 50$. In general the plots show the noise reduction due to the emitter degeneration. For a very strong emitter degeneration, the normalized limiting and excess noise components approach the asymptotic values $(2/\beta)^{1/2}$ and $(2)^{1/2}$, respectively.

For $b = d = 0$, i.e., for an ideal dissipationless current mirror, the noise components become just $\sqrt{2}\, I_{cs}$ and $\sqrt{2}\, I_{bx}$, where the $\sqrt{2}$ accounts for the rms addition of both transistor noise sources.

For the important case of a current mirror without emitter degeneration, (25) and (26) reduce to

$$(I_{ol})_{d=0} = \sqrt{2}\, I_{cs} \frac{(1 + 2b + b^2/\beta)^{1/2}}{1 + b/\beta} \tag{27}$$

$$(I_{ox})_{d=0} = \sqrt{2}\, I_{bx} \frac{[1 + (mb)^2]^{1/2}}{1 + b/\beta}. \tag{28}$$

Expressions (27) and (28) are plotted in Fig. 6(a) for the range $0.1 \leqslant b \leqslant 50$ and for some typical values of β and m. Although in all cases both noise components increase with r_b, the degradation of the limiting and excess noise components due to $r_b \neq 0$ is below 3 dB for $b < 1/2$ and $b < 1/m$, respectively. In other words, decreasing the value of b below these limits only provides a negligible reduction in the output noise.

As far as the noise dependence on the bias current I_o is concerned, (27) and (28) show that both noise components should decrease with I_o due to the simultaneous decrease of b and I_{cs} or I_{bx}. Normalized plots of I_{ol} and I_{ox} as a function of the bias current are shown in Fig. 6(b) and (c).

IV. Noise Reduction Due to Degeneration

The noise components I_{ol} and I_{ox} given by the complete expressions (25) and (26) are plotted in Fig. 7(a) and (b) as a function of the degeneration parameter d for different values of b and for typical values of β and m. These graphs clearly show that in most cases both noise components decrease with increasing d down to a minimum value. The noise reduction is due to the circuit transconductance reduction in Fig. 5, and the flattening effect to the simultaneous increase of the equivalent noise voltages. The addition of emitter degeneration resistances to a current mirror source appears then as a simple means to improve the noise performance. Apart from this effect, emitter degeneration also increases the output resistance, improves the matching, and reduces the maximum operating voltage range of the current source.

The noise improvement can be better evaluated by introduc-

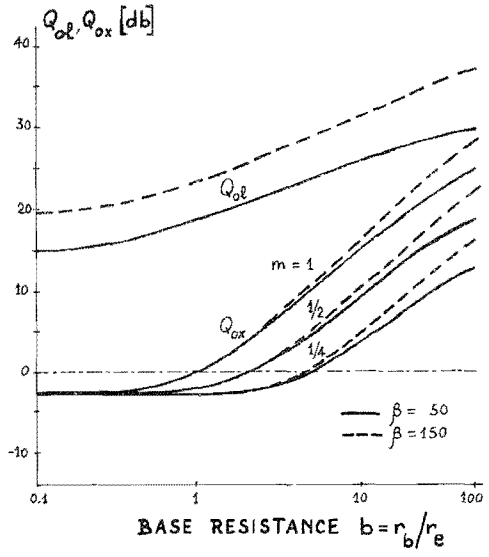

Fig. 8. Noise reduction factors Q_{ol} and Q_{ox} as a function of the base resistance parameter b. These factors measure the maximum noise reduction due to a strong emitter degeneration and are equal to the ratio of the initial and asymptotic values in Fig. 7(a) and (b).

ing the factors Q_{ol} and Q_{ox}

$$Q_{ol} = (I_{ol})_{d=0}/(I_{ol})_{d\to\infty}, \qquad Q_{ox} = (I_{ox})_{d=0}/(I_{ox})_{d\to\infty} \tag{29}$$

which measure the maximum noise reduction afforded by a strong emitter degeneration. From (25) and (26), Q_{ol} and Q_{ox} become

$$Q_{ol} = (1 + b/\beta)^{-1}\left[\frac{\beta(1+2b)+b^2}{2}\right]^{1/2} \tag{30}$$

$$Q_{ox} = (1 + b/\beta)^{-1}\left[\frac{1+(mb)^2}{2}\right]^{1/2}. \tag{31}$$

These factors are plotted as a function of b in Fig. 8. Within the limits shown in Fig. 8 the emitter degeneration appears to be more effective in reducing the limiting noise than the excess noise. Moreover, in the first case a reduction occurs for any value of b including $b = 0$, while in the second one a reduction occurs only when $b > 1/m$, i.e., when $r_b I_o > kT/mq$.

In general, the total noise reduction Q_{on} becomes Q_{ol} or Q_{ox} when the noise bandwidth is fully located in the shot or in the excess region, respectively. When the noise bandwidth overlaps both regions, as in typical audio applications, Q_{on} ranges between Q_{ol} and Q_{ox}. This trend is clearly seen in the computed spectral density curves of Fig. 9.

V. Computer-Aided Analysis

The circuit-analysis program SPICE[2] has been used to verify and expand the previous analytical results. The transistor noise model assumed in all noise computations was the complete hybrid π model with noise generators similar to those shown in Fig. 2 and (2)-(5). The excess noise was restricted to a single $1/f$ generator located at $m = 1$ with a spectral density given by (6) where

$$C_a = 6.6 \times 10^{-16}, \qquad \gamma_a = 1. \tag{32}$$

These values were taken from data given by Meyer, Nagel, and Lui [16] for monolithic n-p-n transistors and for a particular process. With these assumptions, the spectral density of the output noise current I_{on} in Fig. 1 was computed in the range 1-50 000 Hz and for $R_E = 0$ and $R_E = 5$ kΩ, where the last value ($d = 200$) approximates with sufficient accuracy the strong emitter degeneration case. Fig. 9(a) and (b) give the results obtained for two values of r_b. In all cases the noise reduction factors Q_{ol} and Q_{ox} derived from the computed plots at the frequency range extremes show good agreement with the values calculated by means of (30) and (31).

A further checking was performed by computing the spot noise currents at 10 Hz for different values of R_E. The

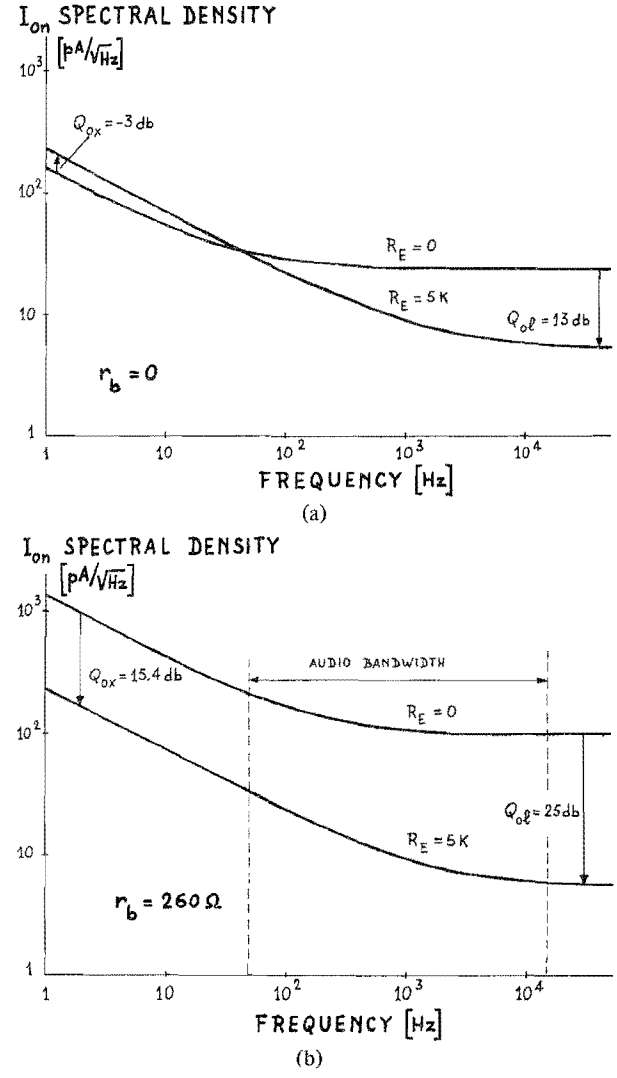

Fig. 9. Computer-derived frequency plots of the total output noise current spectral density for (a) $r_b = 0$ and (b) $r_b = 260\ \Omega$. In all cases, a typical $1/f$ excess noise generator and $I_i = I_o = 1$ mA and $\beta = 50$ are assumed. The downward shift of the $R_E = 5$ kΩ curves at the frequency range extremes represent the noise reduction factors due to a strong emitter degeneration.

[2]SPICE is an IC oriented computer-aided analysis program developed by L. Nagel, University of California, Berkeley.

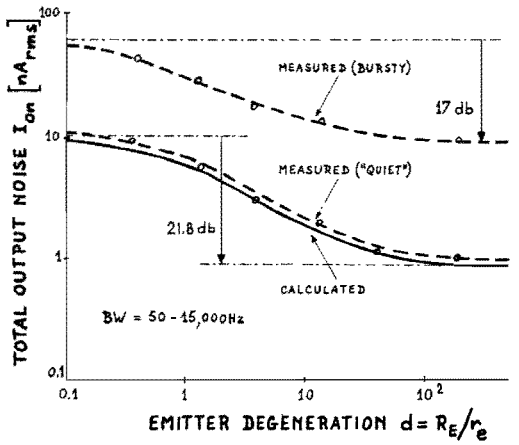

Fig. 10. Wide-band output noise as a function of R_E/r_e for $I_I = I_O = 1$ mA, $\beta = 50$, and $r_b = 260\ \Omega$. The solid line has been calculated by rms integration of several computer-derived spectral density plots similar to Fig. 9(b). The dashed lines give the experimental results obtained with "quiet" and "bursty" monolithic transistors.

normalized results, for $r_b = 250\ \Omega$, are shown as dotted curves in Figs. 6 and 7.

Fig. 10 shows the total output noise for a typical audio bandwidth as a function of the degeneration resistance R_E. This plot was obtained by rms integration of several computed spectral density curves similar to Fig. 9(b).

VI. Experimental Results

The current mirror source of Fig. 1 was implemented with typical monolithic n-p-n transistor pairs and the total output noise current measured for the audio bandwidth 50–15 000 Hz.

The samples used had $20 \times 20\ \mu^2$ emitter area, single base contact, $140\ \Omega/\square$ base resistivity with $r_b \sim 250\ \Omega$ and $\beta = 50$–70 at 1 mA of collector current.

The average results for previously selected lots of "quiet" (burst-noise-free) and bursty transistor pairs are also shown in Fig. 10. Measurements were performed by means of a calibrated bandpass amplifier with a low-noise JFET input stage. The noise voltage developed by the current mirror source across a 20-kΩ load resistor was recorded for different R_E's and constant I_O. The final data were corrected for the residual noise due to the bias and load resistances and the amplifier input stage.

The experimental noise curve obtained with "quiet" transistors follows closely the previously computed curve. This indicates a good fit of the constant values given in (32) to the flicker noise behavior of the particular samples measured. Due to the higher excess noise content of the bursty transistors, the noise reduction due to the degeneration in this case approaches, as expected, the value of Q_{ox} shown in Fig. 9(b).

VII. Other Current Source Topologies

Several improved versions of the basic current mirror source, commonly used in analog IC's, are shown in Fig. 11. In the two-diode current mirror of Fig. 11(a), the additional emitter-follower transistor improves matching at low values of β. The cascode current source of Fig. 11(b) increases the output

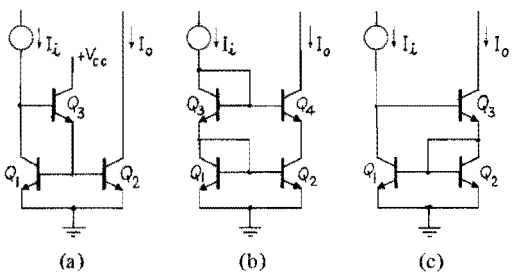

Fig. 11. Other current source topologies. (a) Two-diode with emitter-follower current mirror. (b) Two-diode with cascode output current mirror. (c) Wilson-type current source.

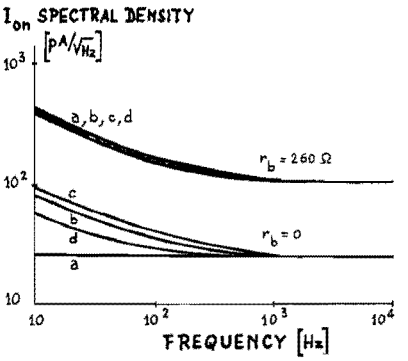

Fig. 12. Computer-derived spectral density plots for the following different current sources. (a) Two-diode with emitter follower [Fig. 11(a)]. (b) Cascode-type [Fig. 11(b)]. (c) Wilson-type [Fig. 11(c)]. (d) Basic current mirror (Fig. 1). In all cases $I_I = I_O = 1$ mA, $R_E = 0$, and $\beta = 50$.

resistance, and the Wilson-type source of Fig. 11(c) [7], [17] improves both the matching and the output resistance. As before, a unity-current ratio and identical transistors are assumed.

A computer-aided analysis of the output current noise of the various current sources of Fig. 11 was performed using the same transistor parameters as in Section VI. The output spectral density curves generated by SPICE are shown in Fig. 12 where for comparative purposes the previous case of the basic current mirror of Fig. 1 is also shown.

These results show that the noise behavior of the four current sources is quite similar, except for the two-diode current mirror of Fig. 11(a) which shows negligible excess noise for $r_b = 0$. This is due to the very low dynamic resistance at the emitter of Q_3 that practically short-circuits the excess current noise generator of Q_1 and Q_2. Unfortunately, this ideal situation is difficult to approximate in practice as it requires $r_b \ll r_e/\beta$.

VIII. Conclusions

The analysis of the noise generated by a unity-ratio current mirror shows that the output limiting and excess noise components decrease with decreasing base resistance although the improvement becomes negligible for $r_b < r_e/2$ and $mr_b < r_e$, respectively. The addition of emitter degeneration resistances provides a simple means to further reduce the output noise. This reduction is more effective for higher r_b/r_e ratios, although the limiting noise can be attenuated $(\beta/2)^{1/2}$ times at

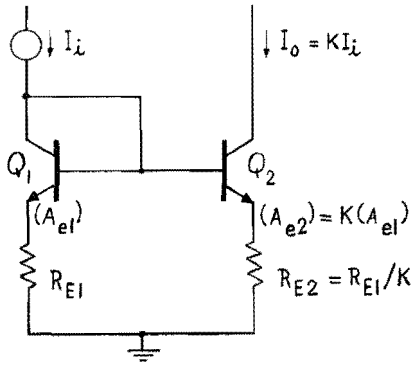

Fig. 13. Current mirror source with ratioed emitter area transistors. The transistor base resistances r_{b1} and r_{b2} are assumed to be related by the matching relation (1A) in the text. The emitter resistors R_{E1} and R_{E2} do not upset the dc current ratio K but only provide an optional emitter degeneration for noise reduction purposes.

$r_b = 0$. On the contrary the excess noise is attenuated by a strong emitter degeneration only for $r_b I_o > kT/qm$.

Assuming transistors with a typical $1/f$ excess noise generator, a CAD noise analysis showed good agreement with the analytical results and measurements performed on "quiet" monolithic transistors. The CAD analysis of the more elaborated current sources of Fig. 11 showed a noise behavior similar to the basic current mirror.

Appendix

Current Mirror Sources with Ratioed Emitter Areas

A current mirror source with a current ratio K defined by the transistor emitter area ratio is shown in Fig. 13, where ratioed emitter degeneration resistors are also included. The output noise current I_{on} generated by this source will be analyzed as in the previous case of Fig. 1 and Section III.

Both transistors in Fig. 13 are assumed identical, modeled by the equivalent circuit of Fig. 2, except for their emitter areas and base resistances which are assumed related through the matching expression

$$K = \frac{I_o}{I_i} \simeq \frac{A_{e2}}{A_{e1}} = \frac{r_{b1}}{r_{b2}} = \frac{R_{E1}}{R_{E2}} = \frac{r_{e1}}{r_{e2}}. \tag{1A}$$

We further assume

$K << \beta$
$\beta \simeq \beta_{dc} >> 1$
A_{e1} = constant for $K \geqslant 1$
A_{e2} = constant for $K \leqslant 1$.

The last two conditions simulate the practical situation where, at constant output, K increases over unity simultaneously with an increase in A_{e2}, and decreases below unity together with an increase in A_{e1}. This suggests the use of r_{b1} and r_{b2} as the independent variables for the $K \geqslant 1$ and $K \leqslant 1$ ranges, respectively.

Identifying with subscripts 1 and 2 the variables associated with Q_1 and Q_2, the noise voltages of Fig. 5, given by (10), (11), (14), (15), and (20) become

$$E_{s1} = (I_{cs})_1 \, (r_{e1} + r_{b1}^2/\beta)^{1/2} \tag{2A}$$

$$E_{x1} = (I_{bx})_1 \, (r_{d1} - m r_{b1}) \tag{3A}$$

$$E_{s2} = (I_{cs})_2 \, [(r_{e2} + r_{b2} + R_{E2} + r_{d1} + R_{E1})^2/\beta + r_{e2}^2]^{1/2} \tag{4A}$$

$$E_{x2} = (I_{bx})_2 \, (m r_{b2} + R_{E2} + r_{d1} + R_{E1}) \tag{5A}$$

$$E_t = (I_{cs})_2 \, [2 r_{e2}(r_{b1} + r_{b2} + R_{E1} + R_{E2})]^{1/2} \tag{6A}$$

and the transconductance given by (18)

$$G_m = [r_{e2} + (r_{d1} + R_{E1} + r_{b2})/\beta + R_{E2}]^{-1}. \tag{7A}$$

Introducing the following parameters

$$b_1 = r_{b1}/r_{e2}, \quad b_2 = r_{b2}/r_{e2}, \quad d = R_E/r_{e2}$$

and using (1A), (2A), (4A), (6A), and (7A), expression (22) yields, after some manipulation

$$I_{ol\,[K \leqslant 1]} = \sqrt{1+K}\,(I_{cs})_2 \cdot \frac{[1 + 2b_2 + b_2^2/\beta + 2d(1 + b_2/\beta) + (1+K)d^2/\beta]^{1/2}}{1 + b_2/\beta + d} \tag{8A}$$

$$I_{ol\,[K \geqslant 1]} = \sqrt{1+K}\,(I_{cs})_2 \cdot \frac{[1 + 2b_1/K + b_1^2/\beta K^2 + 2d(1 + b_1/\beta K) + (1+K)d^2/\beta]^{1/2}}{1 + b_1/\beta K + d} \tag{9A}$$

where (9A) is just (8A) with b_1/K substituted for b_2.

Expressions (8A) or (9A) give the limiting noise current as a function of K for any fixed b_1 or b_2, respectively. The first is useful for the noise evaluation at constant output in the range $K \leqslant 1$, and the second in the range $K \geqslant 1$. For $K = 1$ and $b_1 = b_2 = b$, both expressions merge into the unity-ratio case given by (25).

Expressions (8A) and (9A), normalized with respect to the unity-ratio case, are plotted in Fig. 14 for different values of b_1, b_2, and for the fixed parameters shown.

Using (1A), (3A), (5A), and (7A) in (23) and proceeding in a similar way, the excess noise becomes

$$I_{ox\,[K \leqslant 1]} = (I_{bx})_2 \frac{\{K^{(2-\gamma)}\,[1 - b_2(m - 1/\beta)]^2 + [K + b_2(m + K/\beta) + (1+K)d]^2\}^{1/2}}{1 + b_2/\beta + d} \tag{10A}$$

$$I_{ox\,[K \geqslant 1]} = (I_{bx})_2 \frac{\left\{K^{(2-\gamma)}\left[1 - \frac{b_1}{K}(m - 1/\beta)\right]^2 + \left[K + \frac{b_1}{K}(m + K/\beta) + (1+K)d\right]^2\right\}^{1/2}}{1 + b_1/\beta K + d} \tag{11A}$$

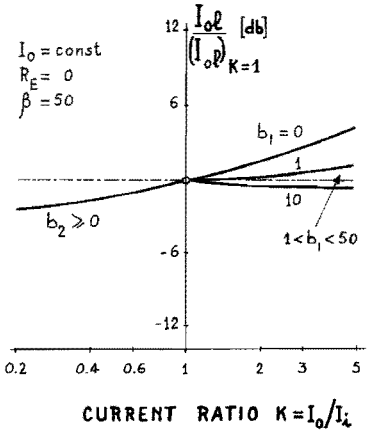

Fig. 14. Normalized limiting noise of the current source of Fig. 13 as a function of the current ratio K at constant output, for different values of b_1, b_2, and for $R_E = 0$. The use of two base resistance parameters simulates the practical situation where K increases over unity with A_{e1} and r_{b1} constant, and decreases below unity with A_{e2} and r_{b2} constant.

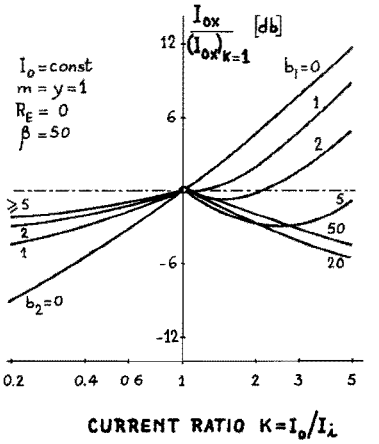

Fig. 15. Normalized excess noise of the current source of Fig. 13 as a function of the current ratio K at constant output for different values of b_1, b_2, and for $R_E = 0$, $m = \gamma = 1$.

where (11A) is just (10A) with b_1/K substituted for b_2.

Expressions (10A) and (11A) give the excess noise current as a function of K for any fixed b_1 or b_2, respectively. For $K = 1$, $b_1 = b_2 = b$ and $m\beta >> 1$, both expressions merge, after some manipulation, into the unity-ratio case given by (26).

Expressions (10A) and (11A), normalized to the case of unity ratio, are plotted in Fig. 15 for the fixed parameters shown.

Figs. 14 and 15 show that both noise components always decrease for $K < 1$, and within a large range of values of b also decrease for $K > 1$. In other words, the previously treated case of $K = 1$ represents approximately a worst case situation.

Acknowledgment

The authors are indebted to Prof. D. O. Pederson, University of California, Berkeley, for making the SPICE program available to the Faculty of Engineering, University of Buenos Aires, and gratefully acknowledge the valuable suggestions by and discussions with Prof. A. Dams.

References

[1] R. J. Widlar, "Some circuit design techniques for linear integrated circuits," *IEEE Trans. Circuit Theory*, vol. CT-12, pp. 586-590, Dec. 1965.

[2] W. R. Davis and H. C. Lin, "Compound diode-transistor structure for temperature compensation," *Proc. IEEE* (Lett.), vol. 54, pp. 1201-1202, Sept. 1966.

[3] C. R. Hoffman, "Temperature sensitivity of compound diode-transistor structure," *Proc. IEEE* (Lett.), vol. 55, pp. 1233-1234, July 1967.

[4] E. S. Yang, "Small-signal characteristics of the diode-stabilized linear integrated devices," *IEEE J. Solid-State Circuits*, vol. SC-3, pp. 190-193, June 1968.

[5] M. J. Callahan, Jr., "Charts speed the designing of constant current sources," *Electronics*, pp. 92-95, Aug. 17, 1970.

[6] P. E. Allen, "Graphical analysis of matched transistor current sinks/sources," *IEEE J. Solid-State Circuits* (Corresp.), vol. SC-9, pp. 31-35, Feb. 1974.

[7] G. R. Wilson, "A monolithic junction FET–n-p-n operational amplifier," *IEEE J. Solid-State Circuits*, vol. SC-3, pp. 341–348, Dec. 1968.
[8] T. M. Frederiksen, "A monolithic high-power series voltage regulator," *IEEE J. Solid-State Circuits*, vol. SC-3, pp. 380–387, Dec. 1968.
[9] K. G. Schlotzhauer and J. V. Hanson, "An improved multioutput current-controlled source," *Proc. IEEE* (Lett.), vol. 61, pp. 1154–1155, Aug. 1973.
[10] R. C. Jaeger, "A high output resistance current source," *IEEE J. Solid-State Circuits*, vol. SC-9, pp. 192–194, Aug. 1974.
[11] T. M. Frederiksen, "Norton quad amplifier subtracts from costs, adds to design options," *Electronics*, pp. 116–120, Dec. 6, 1973.
[12] J. W. Haslett, "Noise performance of the new Norton op amps," *IEEE Trans. Electron Devices*, vol. ED-21, pp. 571–577, Sept. 1974.
[13] C. D. Motchenbacher and F. C. Fitchen, *Low-Noise Electronic Design*. New York: Wiley, 1973, chs. 4 and 5.
[14] R. C. Jaeger and A. J. Brodersen, "Low-frequency noise sources in bipolar junction transistors," *IEEE Trans. Electron Devices*, vol. ED-17, pp. 128–134, Feb. 1970.
[15] A. J. Brodersen, E. R. Chenette, and R. C. Jaeger, "Noise in integrated-circuit transistors," *IEEE J. Solid-State Circuits*, vol. SC-5, pp. 63–66, Apr. 1970.
[16] R. G. Meyer, L. Nagel, and S. K. Lui, "Computer simulation of $1/f$ noise performance of electronic circuits," *IEEE J. Solid-State Circuits* (Corresp.), vol. SC-8, pp. 237–240, June 1973.
[17] T. J. van Kessel and R. J. van de Plassche, "Integrated linear basic circuits," *Philips Tech. Rev.*, vol. 32, no. 1, pp. 1–12, 1971.

From 1952 to 1958 he worked with Phillips Argentina in the area of industrial and consumer electronic applications. During 1959 he was involved in the research of solid-state devices in the Laboratoire d'Electronique et Physique Appliquées, Paris, France. From 1961 to 1965 he was employed with IBM France where he worked in the area of thin film memories and parametric logic. In 1966 he joined the Sprague Electric Company, North Adams, Mass., where he was engaged in the design and development of analog integrated circuits. He returned to Argentina in 1968, and since then has been a Professor in the Department of Electronics, Faculty of Engineering, University of Buenos Aires, Buenos Aires, Argentina. He is the author of many technical papers.

Mr. Bilotti is a member of the National Academy of Physical Sciences of Buenos Aires, the Asociación Argentina de Electrotécnicos, and the Sociedad Científica Argentina.

Alberto Bilotti (S'45–A'48–SM'65) was born in Bahía Blanca, Argentina, on January 3, 1925. He received the Diploma of Electrical Engineer from the National University of La Plata, La Plata, Argentina, in 1948.

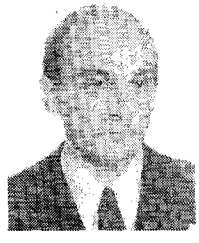

Eduardo Mariani was born in Buenos Aires, Argentina, on November 23, 1944. He received the Diploma of Electromechanical Engineer from the University of Buenos Aires, Buenos Aires, Argentina, in 1972.

He worked on the development of TV receivers for Motorola Argentina in 1963. Since 1964 he has been with the Instrumental Laboratory of the Department of Electronics, Faculty of Engineering, University of Buenos Aires, where he is presently engaged in the design and development of educational equipment, telemetry phase-lock discriminators, and wide-band amplifiers.

Mr. Mariani is a member of the Centro Argentino de Ingenieros.

A Monolithic 8 pJ/2 GHz Logic Family

TSUNETA SUDO, TSUTOMU KAMOTO, HISAKAZU MUKAI, HAJIME SASAKI, MEMBER, IEEE, HIROSHI SHIBA, AND AKIHIKO MORINO, MEMBER, IEEE

Abstract—**A monolithic logic family has been developed for high-speed communication systems usage. Developed logic family affords 8 pJ speed-power product, 2 GHz toggle frequency and 400 ps/gate propagation delay time in 50 Ω transmission systems.**

The primary factor for realizing the high-speed, low-power operation is new circuit configuration: modified nonthreshold logic (NTL). Transistors in this circuit are made to operate almost in the active region. This increases switching speed. In addition, a novel master-slave flip-flop configuration has been designed to operate with propagation delay nearly equal to that of gate.

The device was fabricated by using junction isolated transistors with an emitter stripe width of 2 μ and cutoff frequency of 4 GHz.

This paper describes the circuit design and performance of developed logic family.

Manuscript received April 8, 1975; revised July 9, 1975.

T. Sudo, T. Kamoto, and H. Mukai are with the Musashino Electrical Communication Laboratory, Nippon Telegraph and Telephone Corporation, Tokyo, Japan.

H. Sasaki, H. Shiba, and A. Morino are with the Integrated Circuit Division, Nippon Electric Company, Ltd., Kawasaki, Japan.

I. Introduction

DIGITAL systems, such as digital communication systems or computers, have continuously increased in their speed and capacity. Realization of such high-speed, large-capacity digital systems largely depends on the development of high-speed monolithic logic family. For example, so called subnanosecond logic circuits with propagation delay time less than 500 ps/gate are the most essential components for the highest speed pulse-code modulation (PCM) transmission systems. In these high-speed digital systems, rise in temperature of each device is also an important problem, because devices are compactly laid out in order to minimize the propagation delay time due to interconnections. From these stand points, a high-speed logic family with minimum power dissipation is highly required.

Although there have been reported several high-speed logic circuits [1]–[4], the maximum toggle frequency and mini-